Chapter 18
In Situ Imaging of Zinc with Synthetic Fluorescent Probes

Jiyao Yu and Christoph J. Fahrni

Abstract Small-molecule synthetic fluorescent probes represent powerful tools for interrogating labile zinc pools in biology. Transported into cells through passive diffusion, they are particularly well suited for visualizing dynamic changes of zinc in living systems. When employing fluorescent probes for visualizing biological zinc, there are important limitations that differentiate this approach from quantitative microanalytical techniques. Notably, fluorescent probes engage in a competitive exchange equilibrium with endogenous ligands and proteins and thus detect changes of labile Zn(II) pools rather than total cellular zinc levels. Focusing on design approaches and photophysical concepts, this chapter offers an overview of the most widely employed fluorogenic and ratiometric probes for the detection of Zn(II) in a biological environment, discusses concepts relevant for the design and application of Zn(II)-responsive probes for two-photon excitation microscopy, and outlines current challenges and limitations of their application in biological systems.

Keywords Exchangeable zinc · Fluorescence imaging · Fluorogenic probes · Emission-ratiometric probes · Two-photon excitation microscopy

18.1 Introduction

Cellular zinc levels are regulated through a complex network of subcellular storage sites such as metallothioneins and membrane-localized transporters that control influx and efflux pathways (Kambe et al. 2015; Hara et al. 2017). While a significant fraction of cellular zinc is tightly bound to proteins where it serves as a catalytic

J. Yu · C. J. Fahrni (✉)
School of Chemistry and Biochemistry, Petit Institute for Bioengineering and Bioscience, Georgia Institute of Technology, Atlanta, GA, USA
e-mail: fahrni@chemistry.gatech.edu

T. Fukada, T. Kambe (eds.), *Zinc Signaling*,
https://doi.org/10.1007/978-981-15-0557-7_18

cofactor or structural support, there is increasing evidence that cells also maintain a labile pool of zinc that might be involved in signaling processes (Khan et al. 2014; Vergnano et al. 2014). Synthetic fluorescent probes offer unique opportunities to explore the nature of this exchangeable zinc pool and to advance our understanding of zinc-dependent signaling and regulatory processes in biology (Carter et al. 2014; Fahrni et al. 2017). Due to their lipophilicity and low molecular weight, synthetic probes can passively diffuse across biological membranes to reach cellular targets in a noninvasive manner, thus enabling the visualization of dynamic changes in live cells. A number of Zn(II)-selective fluorescent probes are commercially available and can be employed with conventional fluorescence microscopes available in most cell biology laboratories. As no additional equipment is required, the detection of Zn(II) with fluorescent probes is cost-effective and often the method of choice for assessing cellular zinc levels. However, fluorescent probes do not report on total cellular zinc concentrations, rather, they reflect on the fraction of labile or exchangeable Zn(II) that is buffered by an ensemble of endogenous proteins and bioligands (Maret 2015). Because fluorescent probes inherently engage in a competitive metal exchange equilibrium, the observed response is dependent on the probe interaction, notably the relative affinities and exchange kinetics. For this reason, fluorescence imaging with Zn(II)-selective probes cannot substitute for quantitative imaging techniques such as x-ray fluorescence microscopy or secondary ion mass spectrometry imaging (McRae et al. 2009). Instead, fluorescent probes offer complementary insights into the dynamics of labile Zn(II).

18.2 Fluorogenic Probes

18.2.1 Design Principles and Applications

At a molecular level, fluorogenic probes are composed of an organic fluorophore tethered to a chelator, which triggers a fluorescence increase upon metal ion binding. The photophysical mechanisms that couple the fluorescence output with the metal binding event are diverse but typically involve controlling the photoinduced movement of electrons or protons in a metal ion-dependent fashion. For example, 8-hydroxy-quinoline and 6-methoxy-8-*p*-toluenesulfonamido-quinoline (TSQ), two of the earliest renditions for probing biological zinc, employ a heterocyclic quinoline ring, which serves both as metal coordination site and fluorophore moiety. The donor attached in the 8-position turns the quinoline ring into a bidentate chelator, which forms with Zn(II) a complex with 2:1 stoichiometry (Fig. 18.1) (Fahrni and O'Halloran 1999; Nasir et al. 1999). While the Zn(II) complex is brightly fluorescent, a non-radiative excited state intramolecular proton transfer pathway is likely responsible for quenching of the quinoline emission in the free probe (Lan and Liu 2015). The underpinning photophysical mechanism is best illustrated with a simplified Jablonski diagram as shown in Fig. 18.1b. Upon photoexcitation, the

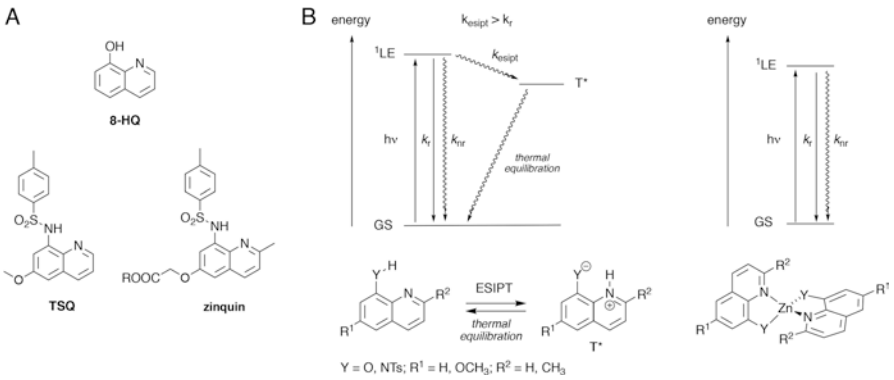

Fig. 18.1 Quinoline-based Zn(II)-selective fluorescent probes. (**a**) Molecular structures of 8-hydroxy-quinoline (8HQ), 6-methoxy-8-*p*-toluenesulfonamido-quinoline (TSQ), and zinquin. (**b**) Simplified Jablonski diagram illustrating the photophysical mechanism for Zn(II)-induced emission enhancement. Excitation of the quinoline fluorophore promotes an exited state intramolecular proton transfer (ESIPT) to yield the zwitterionic tautomer T∗, which thermally equilibrates back to the ground state (GS). In the presence of Zn(II), the bidentate quinoline ligand forms a tetrahedral complex, where ESIPT quenching is no longer possible and the fluorescence is switched on

basicity of the quinoline nitrogen increases concomitantly with the acidity of the neighboring hydroxy or sulfonamide group, thus promoting a proton transfer to yield a zwitterionic intermediate, which then thermally equilibrates back to the original ground state protomer without photon emission. In the complexed form, Zn(II) occupies both the proton donor and acceptor sites, thus inhibiting the original proton transfer quenching pathway and restoring fluorescence of the quinoline fluorophore. Because the quinoline heterocycle acts as a strong photobase in its own right (Hunt and Dawlaty 2018), the fluorescence remains quenched even under basic conditions where the hydroxy or sulfonamide groups are deprotonated. Although other divalent transition metal ions such as Mn(II), Fe(II), or Co(II) can form analogous complexes, their open d-shell electron configuration results in efficient fluorescence quenching.

The selectivity of TSQ for the detection of biological zinc within the chemically complex environment of tissues was corroborated with the neo-Timm stain (Frederickson et al. 1987; Frederickson 1989), a histochemical method based on autometallographic enhancement of zinc selenide nanoparticles formed from histochemically reactive zinc upon perfusion with sodium selenide (Danscher 1981). Such correlative imaging studies were not only critical to validate the observed fluorescence staining pattern but also to promote overall confidence when employing synthetic probes in other biological systems. To increase retention in live cells, Zalewski et al. developed the quinoline derivative zinquin carrying an ester group (Zalewski et al. 1993; Mahadevan et al. 1996). Upon cleavage by cellular esterases, the ester group is converted into a negatively charged carboxylate anion with has a much-decreased membrane permeability.

The early success of quinoline-based probes for the in situ detection of biological zinc stimulated further developments, which evolved into a vibrant area of research that has produced a large body of literature as summarized in several comprehensive reviews (Carter et al. 2014; Jiang and Guo 2004; Kikuchi et al. 2004; Lim et al. 2004; Nolan and Lippard 2009; Xu et al. 2010; Carter et al. 2014; Chen et al. 2015; Chabosseau et al. 2018; Sfrazzetto et al. 2016). While the probes reported thus far cover a broad range of binding affinities and exhibit diverse photophysical characteristics, both in terms of fluorescence contrast and available emission wavelengths, the literature on their biological applications remains comparatively sparse. Because most probes require elaborate multistep synthetic procedures, the majority of biological studies have been conducted with reagents that are available from commercial sources. With these limitations in mind, the following discussion focuses on general guidelines for the application of these reagents rather than reviewing the extensive literature on Zn(II)-responsive fluorogenic probes that are less readily accessible. As a newer development, the design and application of fluorescent probes for two-photon excitation microscopy (TPEM) will also be reviewed, including some of the latest development concerning ratiometric Zn(II)-selective fluorescent probes.

The majority of commercially available Zn(II)-selective fluorescent probes respond with an increase in fluorescence intensity upon saturation with Zn(II) (Table 18.1). With the exception of TSQ and zinquin, all probes employ a xanthene derivative as fluorophore moiety, which is linked to various chelators acting as Zn(II) recognition sites (Fig. 18.2). In contrast to the quinoline-based probes discussed above, the Zn(II)-induced fluorescence switching of xanthene derivatives relies on a photoinduced electron transfer (PET) mechanism rather than excited state proton transfer (Fig. 18.3). Specifically, excitation of the fluorophore promotes an electron into an empty antibonding orbital, and the resulting vacancy in the bonding orbital is filled by accepting an electron from the tethered chelator acting as an electron-rich donor. The resulting radical ion pair undergoes charge recombination to furnish the original ground state, a process that usually occurs through thermal equilibration without emission of a photon. Because Zn(II) coordination lowers the energy of the electron donor, formation of the radical ion pair becomes less favorable, and the driving force for the electron transfer is diminished. As a consequence, radiative deactivation can now effectively compete with PET, which would otherwise quench the fluorescence. Thus, the observed Zn(II)-induced fluorescence enhancement can be rationalized based on the efficiency of PET quenching in the free probe and its inhibition upon Zn(II) binding.

As evident from Table 18.1, different combinations of chelator and fluorophore moieties produce quite different fluorescence contrasts, which directly affect the limit of detection and overall sensitivity. In addition to the magnitude of fluorescence enhancement upon saturation with Zn(II), the limit of detection also depends on the molar brightness, which corresponds to the product of the absorption cross section (molar extinction coefficient) at the wavelength of excitation and the quantum yield of the Zn(II)-bound probe. Probes with higher fluorescence contrast and brightness can be employed at a lower concentration and thus are capable of detect-

Table 18.1 Photophysical and thermodynamic properties of commercially available Zn(II)-selective fluorogenic probes

	Free probe			Zn(II)-bound probe							
Probe	λ_{abs} [nm]	λ_{em} [nm]	Φ_F[a]	λ_{abs} [nm]	ε [b] [10^4 $M^{-1}cm^{-1}$]	λ_{em} [nm]	Φ_F[a]	log$K$ [c]	$\Phi\ \varepsilon$[d]	f_e [e]	References
TSQ	369	535	0.002	369	0.61	535	0.34	7.7	0.2	170	Pearce et al. (2001), Nowakowski et al. (2015), and Radford et al. (2013)
Zinquin acid	336	n.d.	n.d.	361	0.79	484	0.13	13.5[f]	0.1	n.d.	Fahrni and O'Halloran (1999), Zalewski et al. (1993), and Mahadevan et al. (1996)
FluoZin-1	496	515	0.005	496	n.d.	515	n.d.	5.1	n.d.	200	Royzen et al. (2005), and Gee et al. (2002a)
FluoZin-2	495	495	n.d.	495	n.d.	525	n.d.	5.7	n.d.	12	Gee et al. (2002a)
FluoZin-3	491	517	0.005	495	7.1	516	0.43	7.8	3.1	86	Gee et al. (2002b), and Marszalek et al. (2016)
RhodZin-3	550	575	n.d.	550	n.d.	575	n.d.	7.2	n.d.	75	Gee et al. (2002a) and Sensi et al. (2003)
ZnAF-1	492	514	0.022	492	7.4	514	0.23	9.1	1.7	10	Hirano et al. (2000)
ZnAF-2	490	514	0.023	492	7.8	514	0.36	8.6	2.8	16	Hirano et al. (2000)
ZnAF-1F	489	514	0.004	492	7.7	514	0.17	8.7	1.3	43	Hirano et al. (2002)
ZnAF-2F	490	514	0.006	492	7.4	514	0.24	8.3	1.8	40	Hirano et al. (2002))
Zinpyr-1	515	529	0.39	507	8.0	529	0.87	9.2	7.0	1.8	Walkup et al. (2000)
Newport Green DCF	505	535	n.d.	505	8.2	535	n.d.	6.0	n.d.	5	Carter et al. (2014), and Iain Johnson (2010)
Phen Green SK	507	532	n.d.	507	8.6	532	n.d.	n.d.	n.d.	n.d.	Carter et al. (2014) and Iain Johnson (2010)

[a]Fluorescence quantum yield
[b]Molar absorption coefficient at absorption maximum (λ_{abs})
[c]Apparent complex stability constant of the probe-Zn(II) complex
[d]Molar brightness (product of molar absorption coefficient and quantum yield, unit [10^4 $M^{-1}cm^{-1}$])
[e]Fluorescence enhancement factor upon Zn(II) saturation / logβ_2 at pH 7.20

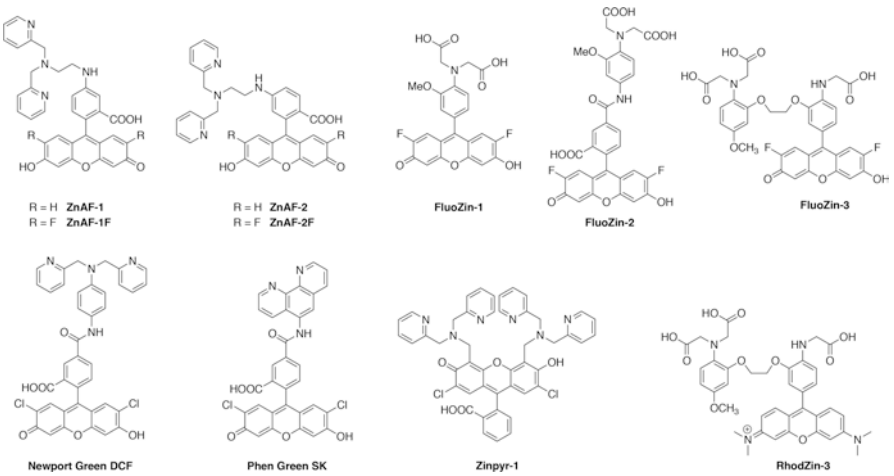

Fig. 18.2 Molecular structures of commercially available Zn(II)-selective fluorogenic probes

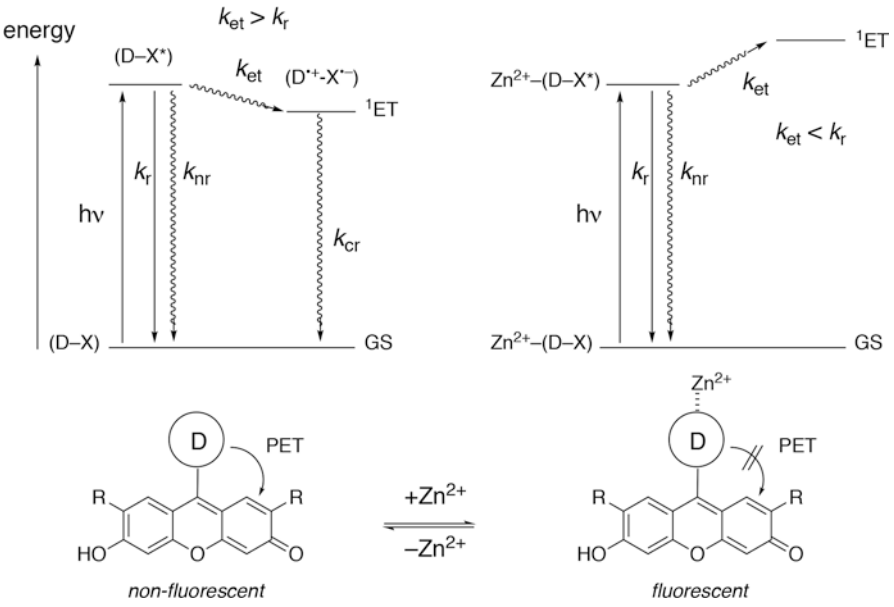

Fig. 18.3 Principle of photoinduced electron transfer (PET) fluorescence switching in xanthene-based Zn(II)-responsive fluorescent probes. Photoexcitation of the xanthene moiety promotes an electron transfer from the nearby donor (D) to yield a radical ion pair ($D^{\bullet+}$-$X^{\bullet-}$), which undergoes non-radiative charge recombination back to the ground state (GS). Because the electron transfer rate constant (k_{et}) is faster than that of radiative deactivation (k_r), the fluorescence is quenched. Upon metal binding to the donor, the electron transfer is rendered less favorable, and radiative deactivation is now the preferred deactivation pathway

ing lower Zn(II) concentrations. Even for the brightest probes, fluorescence intensity measurements with conventional fluorimeters still require probe concentrations in the high nanomolar range to achieve a robust signal-to-noise ratio.

The Zn(II)-selective response of fluorogenic probes can be harnessed to determine the total Zn(II) concentration in analytical samples by fluorimetry. If the Zn(II) dissociation constants of the probe is significantly lower than the total probe concentration, the fluorescence intensity increases with a steady slope upon addition of Zn(II) up to the saturation point. Given this linear relationship, a simple calibration curve can be established and utilized to determine the total Zn(II) concentration of an unknown sample by fluorimetry, provided no other ligands are present that bind Zn(II) with similar or higher affinity than the probe. To exclude such interference, the sample is therefore best digested by boiling with concentrated acid followed by neutralization with base. Following this approach, fluorescent probes are well suited to measure total Zn(II) concentrations in a wide range of samples, including bulk cells or tissues, thus offering a low-cost alternative to microanalytical methods that require expensive instruments such as inductively coupled plasma mass spectrometry (ICP-MS), atomic emission spectroscopy (AES), or total reflection x-ray fluorescence elemental analysis (TXRF) (McRae et al. 2009).

18.2.2 Visualizing Zinc in Cells and Tissues

Due to their lipophilicity and small molecular size, many fluorescent probes can diffuse across lipid bilayers to reach subcellular compartments and organelles in a noninvasive fashion. Although hydrophilic charged probes are usually not membrane-permeant, they are useful for detecting extracellular analytes as demonstrated, for example, with the dynamic release of Zn(II) ions from pancreatic β-cells (Gee et al. 2002b). To enable cellular uptake and increased retention, fluorescent probes containing carboxylic acids can be masked as ester derivatives, an approach that was pioneered by Tsien and coworkers in the early 1980s (Tsien 1981). Upon cellular uptake, the ester group is cleaved by nonspecific cytosolic esterases to release the negatively charged carboxylate anion, thus rendering the probe membrane impermeant and increasing its overall cellular retention. Due to more favorable hydrolysis kinetics, acetoxymethyl (AM) esters are preferred over methyl or ethyl ester derivatives, and most of the carboxylic acid-containing probes listed in Table 18.1 are also commercially available as AM ester derivatives. When using AM esters for live cell imaging studies, the cell culture medium can be supplemented with millimolar concentrations of pyruvate to counteract potential toxicity of formaldehyde, which is a by-product of the AM ester hydrolysis (Tsien and Pozzan 1989). While AM ester derivatives have been widely used for cellular in vitro studies, high levels of extracellular esterases in the vascular space may cleave the probe prior to cellular uptake, thus rendering AM derivatives ineffective for monitoring intracellular processes in vivo (Jobsis et al. 2007). Altogether, the ability to mask charged probes and deliver them into the cytosol of live cells permitted for the first

time the noninvasive observation of various metal ions, a key development that revolutionized cell biology research.

Analogous to the fluorimetric analysis of bulk samples, the intracellular concentration of a fluorescent probe must be sufficiently high to achieve a robust signal-to-noise ratio for fluorescence imaging. The following consideration provides a rough estimate for the lower limit of the cellular fluorophore concentration. Assuming an average focal volume of around 1 fL for a confocal imaging setup, a single probe molecule placed within this volume would yield a nominal concentration of 1.7 nM. Because the emission of a single fluorophore would be obscured by the autofluorescent background within a cellular environment, the probe must be present at significantly higher concentration, thus placing the recommended loading into the high nano- to low micromolar concentration window.

The first fluorescent probes for imaging metal ions in live cells were geared toward monitoring intracellular Ca(II) and Mg(II) fluxes, which occur at concentrations that are significantly higher than the typical cellular loading levels of the probe. Under these conditions, the analyte concentration is not limiting, and the fluorescence response toward increasing metal ion concentrations follows a sigmoidal binding isotherm centered around the probe K_d (Fig. 18.4). As these probes engage with the metal ion in a 1:1 binding equilibrium, the fractional saturation f, defined as the ratio of the metal-bound to total probe concentration, is a direct measure of the free metal ion concentration according to Eq. (18.1):

$$f = \frac{[\mathrm{M}]}{K_d + [\mathrm{M}]} \tag{18.1}$$

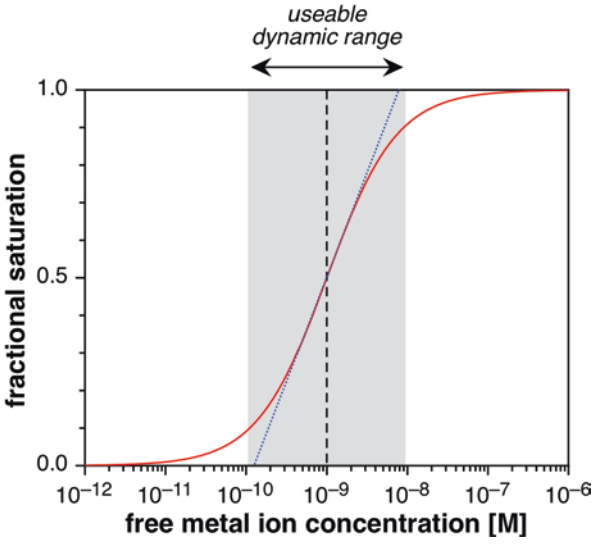

Fig. 18.4 Binding isotherm for a probe-metal complexation equilibrium with 1:1 stoichiometry assuming a complex dissociation constant (K_d) of 1 nM. The shaded area indicates the free metal ion concentration range where the fractional saturation of the probe resides between 10 and 90%. As illustrated with the dotted blue trace, a linear approximation of the probe response is only valid for metal ion concentrations close to the probe K_d

Conversely, the above relationship can be used to calculate the free metal ion concentration based on the fractional saturation of the probe after solving for [M]:

$$[\mathrm{M}] = \frac{K_d f}{f - 1} \tag{18.2}$$

Based on Eq. (18.1), it is apparent that the fractional saturation of the probe is 50% if the free metal ion concentration is equal to the K_d. Because the slope of the binding isotherm is the steepest within one logarithmic unit below and above the K_d, the dynamic range window of the probe is limited to approximately two decades centered around the K_d (shaded area in Fig. 18.4). Because the concentration of the probe-metal complex is significantly lower than the total metal concentration, the fractional probe saturation represents a direct measure of the cellular metal status.

The success of these early studies stimulated the development of fluorescence probes for other biologically relevant metal ions, including zinc (Maret 2015). However, there is an important difference that must be taken into consideration when employing Zn(II)-selective fluorescent probes. Although total cellular zinc levels may approach low millimolar concentrations, a significant portion of zinc remains buried within the binding pockets of proteins and is therefore not accessible, even for probes with much tighter binding affinities. Unlike Ca(II) and Mg(II), which rapidly equilibrate within the cytosol, only a fraction of the total cellular Zn(II) is exchangeable and can be detected with a fluorescent probe. Increasing evidence suggests that this labile, exchangeable zinc pool is buffered at high pico- to low nanomolar concentrations (Qin et al. 2011; Vinkenborg et al. 2009; Hessels and Merkx 2014), presumably involving an ensemble of proteins such as metallothioneins and low-molecular-weight bioligands (Colvin et al. 2010). Although the actual buffer depth, which corresponds to the total concentration of exchangeable Zn(II), is not known, it likely resides in the tens of micromolar range and thus should be sufficient to saturate a probe that is present at low micromolar concentrations. Provided the probe K_d matches the buffer window of the exchangeable Zn(II) pool, the fractional saturation can still be used as an indicator of the cellular zinc status as discussed above. However, it is important to note that there is no linear relationship between the probe response and *total* cellular Zn(II) concentration; instead, the probe only reports on changes in buffered levels. For this reason, in-cell analysis of the fluorescence response of a probe cannot be used as a substitute for measuring total Zn(II) levels by bulk analytical methods such as ICP-MS or AES.

The tight buffering of the exchangeable Zn(II) pool has another important implication when employing fluorescent probes. Because the buffered Zn(II) levels are several orders of magnitude lower than the probe concentration, the Zn(II) exchange kinetics would be exceedingly slow if the probe could only access free aquated Zn(II) ions. In view of the short experimental equilibration times, the exchange of Zn(II) between endogenous ligands and the probe likely occurs through an associate mechanism involving a transient ternary complex. Because the kinetics for formation of the ternary complex is expected to depend on both the electrostatic and steric

nature of the probe and the coordination environment of the endogenous Zn(II) sites, it is conceivable that structurally different fluorescent probes might produce different results, even if their Zn(II)-binding affinities are identical. Such differences might be especially pronounced when acquiring data with protein-based genetically encoded vs. small synthetic fluorescent probes (Qin et al. 2013).

18.2.3 Limitations and Artifacts

When employing fluorogenic probes for monitoring cellular Zn(II) levels, it is important to keep in mind that the observed fluorescence signal is only an indirect measure that might be influenced by factors other than Zn(II). For example, changes in environmental polarity might trigger a fluorescence increase without binding of the target analyte. This is especially of concern for probes that employ a PET switching mechanism because the charge-separated radical intermediate is destabilized in a low polarity environment such as lipid bilayers (Fahrni et al. 2003). Even without polarity-induced fluorescence increases, accumulation of a fluorogenic probe within a compartment leads to a fluorescence enhancement due to the background fluorescence of the unbound probe. It is quite common that synthetic fluorescent probes exhibit an uneven cellular distribution. Depending on the molecular size and polarity, they often localize to specific subcellular structures and compartments. For example, the fluorescence staining pattern of zinquin in untreated HeLa cells appeared uniform with a mostly cytosolic distribution (Devergnas et al. 2004), while FluoZin-3 localized to the Golgi apparatus (Qin et al. 2013), and Zinpyr-1 was sequestered mostly into mitochondria (Lu et al. 2016). Thus, accumulation within subcellular compartments, partitioning into lipid bilayers, or association with lipid droplets might produce bright staining by the free probe alone, thus leading to potential imaging artifacts. To avoid misinterpretations, the reversibility of the fluorescence signal is best tested with a membrane-permeant high-affinity chelator such as TPEN. Ternary complex formation by association with proteins (Meeusen et al. 2012; Karim and Petering 2016) or low-molecular ligands (Staszewska et al. 2013; Marszalek et al. 2018) might present another source of potential artifacts. For example, detailed subcellular fractionation studies of cell lysate revealed that TSQ and zinquin (Fig. 18.1) form both ternary adducts with zinc proteins (Nowakowski et al. 2015). Rather to competitively chelate Zn(II) from proteins, the probes form ternary adducts, which in fact appear to be the major source of the observed fluorescence staining in cells.

18.3 Ratiometric Fluorescent Probes

Developed more than 30 years ago for the visualization of calcium ion fluxes (Grynkiewicz et al. 1985), ratiometric probes respond with a spectral shift rather than a large intensity increase upon binding of the analyte. Due to this spectral shift, the ratio of fluorescence intensities at two different wavelengths is different for the free and metal-bound probe but independent of the probe concentration, thus rendering ratiometric microscopy less prone to artifacts than intensity-based imaging with fluorogenic probes. Furthermore, the intensity ratio can be directly related to the actual buffered metal ion concentration [M] according to Eq. (18.3) (Tsien 1988):

$$[\mathrm{M}] = K_d \left(\frac{R - R_{\min}}{R_{\max} - R} \right) \left(\frac{S_\mathrm{f}}{S_\mathrm{b}} \right) \tag{18.3}$$

where K_d is the dissociation constant of the metal-bound indicator, $R_{\min}$ and $R_{\max}$ are the minimum and maximum intensity ratios for the free and metal-bound indicator, and S_f and S_b are instrument-dependent calibration constants. The instrument-dependent term $S_\mathrm{f}/S_\mathrm{b}$ becomes obsolete if one of the acquisition wavelengths is chosen at the crossover point of the calibration spectra. In this case, the limiting ratio values $R_{\min}$ and $R_{\max}$ can also be used to determine the fractional probe saturation f for a given intensity ratio R according to Eq. (18.4):

$$f = \frac{R - R_{\min}}{R_{\max} - R_{\min}} \tag{18.4}$$

where f is defined as the ratio of the metal-bound and total probe concentrations. The dissociation constant K_d is best determined from an independent calibration using fluorescence intensity data at a single wavelength. It is also important to note that Eq. (18.3) is only valid if the probe engages with the metal ion in a simple 1:1 complexation equilibrium, both in calibration media and within the chemically complex environment of cells.

As the ratiometric probe must be present at low micromolar concentrations to produce an adequate fluorescence signal over cellular background, it raises the question of how this approach can be used to detect Zn(II) at nanomolar levels and below. Instead of capturing free aquazinc(II) ions, the probe engages in a competitive exchange equilibrium with endogenous Zn(II) ligands, likely through an associative mechanism as described in Sect. 18.2. Thus, the probe affinity dictates to what degree Zn(II) can be chelated from this pool. Upon equilibration, the fractional saturation of the probe, which can be derived from the intensity ratio, reflects the thermodynamic availability of cellular Zn(II) based on the isotherm shown in Fig. 18.4. As long as the buffer depth, corresponding to the total concentration of exchangeable Zn(II), is significantly larger than the probe concentration, the ratio-

metric probe response is expected to accurately reflect the cellular zinc status. As the buffer depth might vary significantly with the cellular zinc status, ratiometric probes should be employed at the lowest possible concentration where a satisfactory signal over background ratio can be achieved. If the probe concentration exceeds the buffer capacity, the resulting fractional saturation no longer reflects the buffered levels. Such probe overloading is particularly of concern when using acetoxymethyl (AM) ester derivatives, which yield increased cellular retention but might produce higher than desired intracellular probe concentrations (Thompson et al. 2012).

Compared to fluorogenic probes, the body of literature on Zn(II)-responsive ratiometric probes is much smaller. An overview of various designs is shown in Fig. 18.5 and the corresponding photophysical properties are compiled in Table 18.2. FuraZin and IndoZin were both derived from the established Ca(II)-selective indicators fura-2 and indo-1 (Gee et al. 2002a). By truncating the original BAPTA ligand, the affinity for Ca(II) was significantly reduced; however, the Zn(II)-binding affinities are too weak for monitoring cytosolic Zn(II) levels, which are buffered at in the low nanomolar range (vide infra). Similarly, ZnAF-R2 was derived from the molecular framework of the Ca(II) probe fura-2 (Maruyama et al. 2002). Although the *N*,*N*-di(2-picolyl)ethylenediamine (DPEN) moiety increases the Zn(II) affinity by approximately tenfold over FuraZin, it still remains too low for accessing endogenous Zn(II) pools. In contrast, the Zn(II) affinity of Zinbo-5 is well matched for biological applications (Taki et al. 2004). The probe responds with a 36 nm red-shift of the emission as Zn(II) coordination displaces the phenolic proton. The coumarin-based probe ZnIC revealed a significant shift of the emission maximum upon saturation with Zn(II) (Komatsu et al. 2007). Employed in live HEK293 cells as well as rat hippocampal slices, the probe revealed dynamic changes of labile Zn(II) availability. The structurally related probe DPA-COUM-4 showed a Zn(II)-induced shift of the absorption and emission maximum; however, the probe was only character-

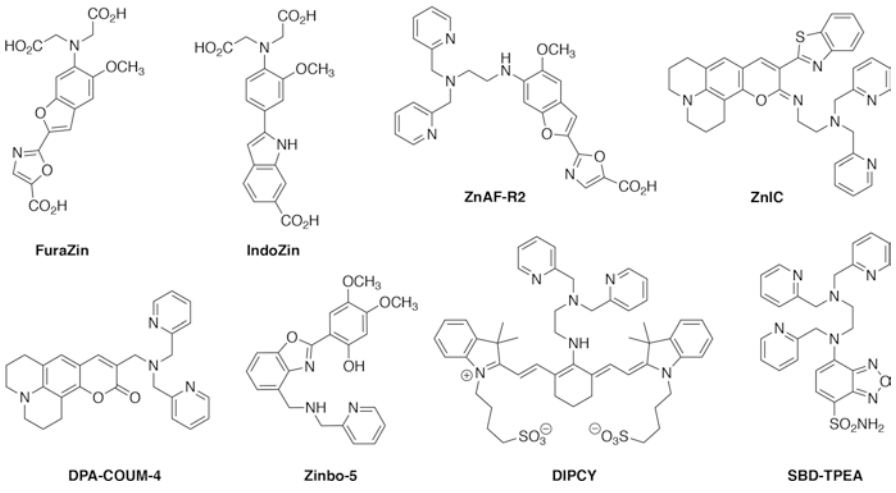

Fig. 18.5 Molecular structures of Zn(II)-selective ratiometric fluorescent probes

Table 18.2 Photophysical and thermodynamic properties of ratiometric Zn(II)-responsive fluorescent probes

	Free probe		Zn(II)-bound probe				
Probe	λ_{abs} [nm]	λ_{em} [nm]	λ_{abs} [nm]	λ_{em}][nm]	log$K$	R_{max}/R_{min}	References
FuraZin	378	510	339	510	5.7	9.0	Gee et al. (2002a)
IndoZin	350	480	350	395	5.5	n.d.	Gee et al. (2002a)
ZnAF-R2	365	495	335	495	6.6	7.0	Maruyama et al. (2002)
ZnIC	513	543	524	558	11.9	2.4	Komatsu et al. (2007)
DPA-COUM-4	400	484	431	505	6.3	n.d.	Lim and Bruckner (2004)
Zinbo-5	337	407	376	443	8.7	33	Taki et al. (2004)
DIPCY	627	758	671	765	7.6	1.5	Kiyose et al. (2006)
SBD-TPEA	456	585	386	545	8.7	1.7	Liu et al. (2014)

ized in methanol and not further tested within a biological system (Lim and Bruckner 2004). Specifically designed for NIR imaging, the cyanine derivative DIPCY responded with a strong shift of the maximum excitation wavelength upon saturation with Zn(II). With a K_d around 2.1 nM (log$K$ = 8.7), the tris-picolylamine derivative SBD-TPEA offers an affinity that is well matched for biological applications as demonstrated for ratiometric imaging of labile Zn(II) in HepG2 cells as well as zebrafish embryos (Liu et al. 2014).

18.4 Fluorescent Probes for Two-Photon Excitation Microscopy

18.4.1 Design Principles and Applications

Originally developed by Webb and coworkers (Denk et al. 1990), two-photon excitation microscopy (TPEM) employs an ultrafast-pulsed laser as excitation source to promote simultaneous absorption of two photons by the fluorophore. Compared to conventional fluorescence imaging, only half of the photon energy is required to reach the same excited state manifold of the fluorophore, thus shifting the excitation window toward the near-infrared region. The shift to longer-wavelength excitation is particularly advantageous for intravital imaging as it results in increased penetration depth, decreased cellular autofluorescence, and reduced phototoxicity (Schießl and Castrop 2016). Because the two-photon absorption process scales with the square of the incident light intensity, the focal volume is significantly smaller compared to one-photon excitation. As a result, only fluorophore molecules that reside near the focal plane are excited, thus yielding intrinsic 3D imaging capabilities and

enabling live cell imaging studies over extended periods by minimizing photobleaching (Schießl and Castrop 2016).

While most established fluorescent probes can be used for TPEM, their relative brightness might be significantly different. In analogy to one-photon excitation, the fluorophore brightness in TPEM depends on the quantum yield and absorption cross section; however, as the quantum mechanical selection rules that govern the two-photon absorption process are different from those for linear absorption, not all fluorophores are equally well-suited for TPEM. A compilation of the two-photon absorption properties for a selection of commonly employed fluorophores and fluorescent probes is shown in Table 18.3. An extensive list of two-photon probes and their 2PA maxima, molecular brightness, and emission ranges has been recently reported by Fiole and coworkers (Ricard et al. 2018). To better compare the one- and two-photon excited fluorescence properties across the different fluorophores, their relative brightness has been normalized to fluorescein as a reference. Among the tabulated fluorophores, rhodamine 6G provides the greatest detection sensitivity in both excitation modes. While the brightness of Alexa Fluor 488 and BODIPY 492 is similar compared to fluorescein, the two-photon excited fluorescence output is significantly attenuated due to the lower 2PA cross sections. In contrast, the cyanine dye Cy5.5 is 35% brighter compared to fluorescein in two-photon excitation mode. Genetically encoded fluorescent proteins such as EGFP (enhanced green fluorescent protein) are particularly attractive for labeling proteins in live cells and whole organisms. A wide variety of fluorescent proteins with emission maxima across the entire visible spectrum are available, and most of them offer a two-photon excited brightness comparable or better than fluorescein (Drobizhev et al. 2011). In general, the two-photon absorption cross section of fluorophores with absorption maxima in the UV range is significantly lower. For example, the brightness of the Ca(II)-responsive fluorescent probes fura-2 or indo-1 is less than 10% compared to fluorescein and decreases even further upon saturation metal binding (Table 18.3). The low two-photon absorption cross section is due to the smaller size of the conjugated π-system, which limits both the oscillator strength and the magnitude of the excited state dipole moment. Nevertheless, the two-photon excited brightness of such dyes is often significantly increased at wavelengths below the 680 nm limit of pulsed Ti:sapphire lasers commonly used in TPEM. For example, the UV-excitable nuclear stain DAPI is approximately tenfold brighter using two-photon excitation at 590 nm compared to excitation above 700 nm using the same laser power (Tragardh et al. 2015).

The theoretical principles that govern the two-photon absorption cross section of a fluorophore are well established (Albota et al. 1998; Rumi et al. 2000), and several comprehensive reviews have been published that summarize various design approaches for fluorophores with high two-photon absorption cross sections and their application in biological systems (Sumalekshmy and Fahrni 2011; Huang et al. 2010; Kim and Cho 2011; Yao and Belfield 2012; Sarkar et al. 2014; Kim and Cho 2015; Liu et al. 2017). At a fundamental level, the two-photon absorption cross section is proportional to the imaginary part of the second-order hyperpolarizability, which increases with increasing excited state polarization. In the simplest case, the

Table 18.3 Two-photon absorption properties of fluorophores and fluorescent probes adopted from linear microscopy

	One-photon abs		Two-photon abs				Rel. brightness[a]			
Probe	λ_{abs} [nm]	ε [10^4 $M^{-1}cm^{-1}$]	λ_{abs} [nm]	δ [b] [GM]	λ_{em} [nm]	Φ_f [c]	1P	2P	Solvent	Ref.
Fluorescein	490	7.6	790	47	520	0.93	1.00	1.00	H_2O, pH 11	Makarov et al. (2008) and Sjoback et al. (1995)
Alexa Fluor 488	495	7.3	940	33	519	0.92	0.95	0.69	H_2O, pH 11	Mütze et al. (2012)
Rhodamine 6G	530	11.6	700	120	565	0.95	1.56	2.61	H_2O, pH 11	Albota et al. (1998) and Kubin and Fletcher (1982)
BODIPY 492	500	7.9	920	15	509	0.95	1.06	0.31	Ethanol	Mütze et al. (2012) and Loudet and Burgess (2007)
Cy3	550	15.0	700	140	565	0.04	0.08	0.13	PBS	Albota et al. (1998) and Mujumdar et al. (1993)
Cy5.5	675	25.0	1280	210	702	0.28	0.99	1.35	PBS	Kobat et al. (2009) and Umezawa et al. (2009)
Fura-2	362	2.7	750	12	512	0.23	0.09	0.06	HEPES, pH 7	Grynkiewicz et al. 1985 and Wokosin et al. (2004)
Fura-2 + Ca(II)	335	3.3	750	1	505	0.49	0.23	0.01	30 mM MOPS	Grynkiewicz et al. 1985 and Wokosin et al. (2004)
Indo-1	349	3.4	730	4.5	485	0.38	0.18	0.04	100 mM KCl	Grynkiewicz et al. 1985, Xu and Webb (1996), and Wang and Yeh (2012)
EGFP	492	4.6	927	39	510	0.76	0.49	0.68	H_2O, pH 8	Drobizhev et al. (2011)

[a]Brightness for one- (1P) and two-photon (2P) excited fluorescence emission relative to fluorescein, calculated as the product of absorption cross section and quantum yield. [b]Two-photon absorption cross section at the wavelength indicated in column to the left. [c]Fluorescence quantum yield

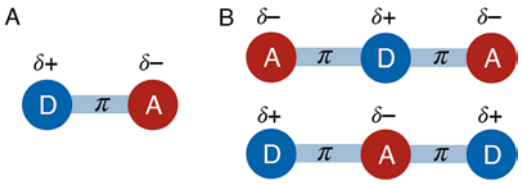

Fig. 18.6 Fluorophore architectures for achieving high two-photon absorption cross sections. (**a**) Simple non-centrosymmetric dipolar arrangement of an acceptor (A) and donor (D) moiety to a fluorophore π-system (π). (**b**) Centrosymmetric architectures with a central donor (top) or acceptor (bottom) moiety

degree of intramolecular charge transfer (ICT) or excited state polarization can be enhanced by modifying the π-system of a linear fluorophore with an electron-rich donor (D) and an electron-deficient acceptor (A) group (Fig. 18.6A). Although such fluorophores are already polarized in the ground state, photoexcitation results in further charge redistribution from the donor to acceptor end of the π-system, thus yielding a strong enhancement of the dipole moment in the excited state compared to the ground state. By extending the fluorophore π-system from a dipolar to a centrosymmetric quadrupolar structure (Fig. 18.6B), very large 2PA cross sections can be achieved (Rumi et al. 2000). While the increase in excited state polarization is beneficial for achieving a high 2PA cross section, it might also have an adverse effect on the quantum yield, especially in polar solvents due to enhanced non-radiative deactivation pathways promoted through stronger solvent-solute interactions. For this reason, enhancing the excited state polarization might in fact yield a fluorophore with lower overall brightness when employed in TPEM.

Although several Zn(II)-selective probes have been employed in TPEM (Khan et al. 2014; Lee et al. 2016; Chang et al. 2004), only few have been specifically designed to achieve a large 2PA cross section. For example, the fluorogenic probe AZn2 takes advantage of the favorable two-photon absorption properties of the donor-acceptor substituted naphthalene derivative acedan (2-acetyl-6-(dimethylamino)naphthalene) (Kim et al. 2008). The probe exhibits an emission maximum at 499 nm and responds with an approximately 50-fold increase in fluorescence intensity, likely mediated through a photoinduced electron transfer switching mechanism as described above for fluorescein-based probes (Fig. 18.7). With a two-photon absorption cross section of 140 GM at 780 nm and a quantum yield of 0.49 for Zn(II)-bound form, the brightness of AZn2 is more than twofold higher compared to fluorescein when used in TPEM. Functionalized with a *N*,*N*-di(2-picolyl)ethylenediamine (DPEN) moiety as Zn(II)-receptor site, the probe offers a Zn(II) dissociation constant of 1.1 nM (pH 7.2, 0.1 M KCl), which is well matched for imaging labile Zn(II) pools within biological systems. Upon incubation in acute hippocampal slices, AZn2 revealed elevated fluorescence in the stratum lucidum of the CA3 region and the hilus of the dentate gyrus, areas that are both known to contain elevated levels of mobile Zn(II) based on histochemical detection (Cole et al. 1999). As an extension of this design, structural modifications of the chelating moi-

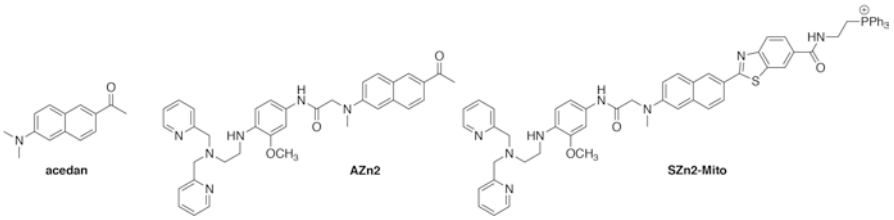

Fig. 18.7 Zn(II)-selective fluorogenic probes for two-photon microscopy employing donor-acceptor substituted naphthalene π-system as fluorophore

ety yielded a series of Zn(II)-responsive probes covering an extended range of dissociation constants from 8 nM to 12 μM while offering similar photophysical properties (Danish et al. 2011). Replacing the acetyl group with a benzothiazole as acceptor moiety, the fluorescence emission of the structurally related probe SZN2-Mito was red-shifted to 536 nm, and the two-photon absorption cross section increased to 155 GM at 750 nm. By attaching the lipophilic triphenylphosphonium group, SZn2-Mito and the related probe SZn-Mito selectively localized to mitochondria (Baek et al. 2012; Masanta et al. 2011). Interestingly, an analogous probe SZn-C containing a carboxylic acid in lieu of the amide substituent selectively localized to the Golgi apparatus (Singh et al. 2015).

18.4.2 Ratiometric Probes for Two-Photon Microscopy

With the ability to follow dynamic changes of analyte concentrations in a semiquantitative fashion, ratiometric imaging is the preferred choice over simple intensity-based approaches. However, not all ratiometric probes are suitable for TPEM. Although the excitation wavelength of femtosecond-pulsed Ti:sapphire lasers can be tuned over a broad range, it is not possible to switch dynamically between two different wavelengths. Ratiometric TPEM must therefore rely on fluorescent probes that respond with a chromatic shift of the emission rather than excitation maximum. As indicated by the data listed in Table 18.2, Zn(II)-induced shifts of the emission maxima are, however, small for most ratiometric probes. The observed small changes are an intrinsic property of the underlying probe architecture in which the metal receptor also functions as the electron donor of a push-pull fluorophore system. The intramolecular charge redistribution that occurs upon photoexcitation results in partial buildup of a positive charge on the donor moiety. Coulomb repulsion by the bound metal ion thus weakens its interaction with the fluorophore, which therefore adopts a polarized charge transfer state similar to that of the free probe. As weakening of the metal-fluorophore interaction proceeds on a faster timescale than radiative deactivation, emission occurs from the equilibrated excited state with only a small change in energy.

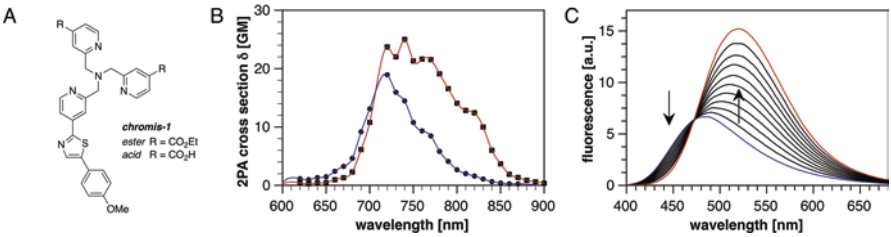

Fig. 18.8 Spectral properties of the ratiometric Zn(II)-selective fluorescent probe chromis-1 (pH 7.0, 10 mM PIPES, 0.1 M KCl, 25 °C). (**a**) Molecular structure of chromis-1 ester and its acid form. (**b**) Two-photon absorption cross section of chromis-1 acid in the free (blue trace) and Zn(II)-saturated (red trace) form. (**c**) Fluorescence emission response upon addition of Zn(II) with 0.1 molar eq aliquots. (Data adopted from ref. (Bourassa et al. 2018). Copyright American Chemical Society 2018)

To design a probe that offers both a large 2PA cross section and a shift of the emission maximum upon metal ion coordination, we devised a push-pull fluorophore architecture where the metal ion receptor is integrated within the acceptor rather than the donor site (Sumalekshmy et al. 2007). With this configuration, the metal-fluorophore interaction is strengthened upon photoexcitation, as it generates a partial negative charge on the acceptor site, thus leading to Coulomb attraction rather than repulsion. Recently implemented in chromis-1 (Fig. 18.8a) (Bourassa et al. 2018), this design approach yielded a large shift of the emission maximum from 483 to 520 nm upon saturation with Zn(II) and a balanced 2PA cross section for the free and Zn(II)-bound forms of 19 and 25 GM, respectively (Fig. 18.8b, c). Despite the small size of the fluorophore π-system, the 2PA action cross section of Zn(II)-bound chromis-1 still approaches 18 GM, corresponding to about 40% of the value for fluorescein.

The acid form of chromis-1 binds Zn(II) with a K_d of 49 ± 13 pM at pH 7.0 (0.1 M KCl, 25 °C). Although other biologically relevant transition metals such as Mn(II), Fe(II), and Co(II) also coordinate to chromis-1, their open d-shell electron configuration leads to fluorescence quenching, likely mediated through energetically low-lying metal-centered d-d states. While chromis-1 acid is not membrane-permeant, the corresponding ethyl ester can readily enter cells. As illustrated by TPEM imaging of live NIH 3 T3 mouse fibroblasts, incubation with chromis-1 ester for 15 minutes in serum-free medium yielded bright fluorescence staining throughout the cytoplasm (Fig. 18.9a). For ratiometric analysis, fluorescence micrographs were acquired by collecting the emission intensity between 425–462 nm (BP1) and 478–540 nm (BP2) with two separate detectors. The corresponding ratio image, which was derived by dividing BP2/BP1, revealed a rather uniform intensity ratio around 0.60 ± 0.16 across all cells (Fig. 18.9a, right). Exposure to a mixture of Zn(II) sulfate and the ionophore pyrithione (ZnPyr) resulted in an immediate increase of the intensity ratio to 2.5 ± 0.6, which was reversed to a slightly lower

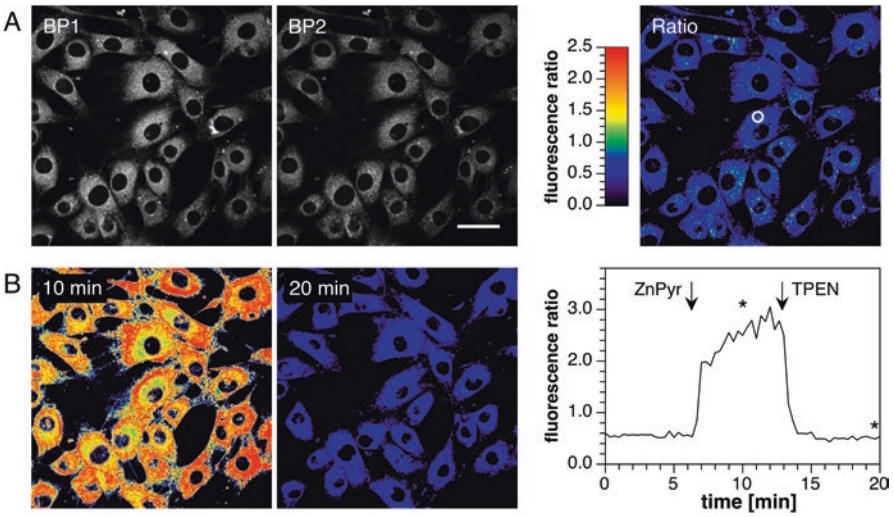

Fig. 18.9 Ratiometric imaging of labile Zn(II) pools in live NIH 3T3 mouse fibroblasts with chromis-1 ester by TPEM (excitation at 720 nm). (**a**) Left: Fluorescence intensity images acquired with 425–462 nm (BP1) and 478–540 nm (BP2) emission channels. Right: Intensity ratio image with R = BP2/BP1. (**b**) Left: Ratio images (BP2/BP1) after addition of 50 μM $ZnSO_4$ and 5 μM pyrithione (ZnPyr), followed by addition of 100 μM TPEN at 13 min. Right: Time course of the average intensity ratio change for the ROI indicated with a white circle in panel A. The asterisks indicate time points for the respective ratio images shown to the left. Scale bar: 40 μm. Data adopted from ref. (Bourassa et al. 2018). Copyright American Chemical Society 2018

value around 0.54 ± 0.13 upon addition of the membrane permeant high-affinity chelator TPEN. A plot of the intensity ratio change as a function of time illustrates the rapid dynamics of Zn(II) binding and competitive chelation by TPEN (Fig. 18.9b, right). Using the K_d of chromis-1 ester (2.4 ± 0.4 nM) and the limiting ratio values after exposure to Zn(II)-pyrithione and TPEN as R_{max} and R_{min}, the fractional saturation of chromis-1 can be calculated with Eq. (18.4) to yield 3–6% under basal conditions. Based on this value, the buffered Zn(II) concentrations reside between 50 and 100 pM, a range that agrees well with previous reports using genetically encoded ratiometric Zn(II) probes (Qin et al. 2011; Vinkenborg et al. 2009; Hessels and Merkx 2014). Chromis-1 was also suitable to visualize dynamic changes of endogenous zinc pools. For example, exposure to the thiol-selective oxidant 2,2′-dithiodipyridine (DTDP) induced a rapid release of Zn(II), presumably from proteins containing sulfhydryl binding sites. Similar to recent observations with a Cu(I)-selective ratiometric fluorescent probe (Morgan et al. 2019), the elevated levels gradually re-equilibrated back to basal conditions. As differences in cellular loading are cancelled out by ratiometric image analysis, this approach is more reliable than intensity-based imaging for monitoring subtle changes in buffered Zn(II) levels. For example, chromis-1 revealed a small but significant decrease in buffered Zn(II) levels upon differentiation of developing into mature oligodendrocytes (Bourassa et al. 2018).

18.5 Conclusions

Since the early success of visualizing histochemically reactive zinc in brain tissue with fluorogenic quinoline derivatives, an extensive range of Zn(II)-responsive fluorescent probes has been developed. The ability to visualize Zn(II) in a noninvasive fashion has provided unique opportunities to unravel the dynamics of biological signaling events in real time. However, there are important limitations that must be carefully considered when employing fluorescent probes in live cells and organisms. First and foremost, fluorescent probes do not report on total zinc levels but only on the exchangeable fraction. The probe dissociation constant should therefore match the buffered concentration of the exchangeable Zn(II) pool. Second, different probes might produce different staining patterns due to variations in subcellular distribution, binding affinity, or pH sensitivity. Third, the response of fluorogenic probes might be susceptible to potential imaging artifacts caused by subcellular sequestration, ternary complex formation with low-molecular-weight ligands, or the association with proteins. In principle, most of these limitations can be addressed by using ratiometric probes; however, only few probes have been developed that offer a dissociation constants within the biologically relevant concentration window, and none of these are commercially available. Moreover, in-cell protein labeling techniques such as HaloTag or SnapTag can readily be adapted to direct synthetic probes to specific subcellular localization (Li et al. 2015; Los et al. 2008; Tomat et al. 2008; Kamiya and Johnsson 2010), thus addressing a key shortcoming over genetically encoded protein-based probes. Regardless of the approach, it is important to keep in mind that fluorescent probes interact with a chemically complex environment and that the identity of the ligands and proteins that participate in buffering labile Zn(II) remains mostly elusive. As the labile Zn(II) pool likely equilibrates through an associate exchange involving ternary complexes (Heinz et al. 2005; Wommer et al. 2002), the underlying kinetic barriers add an additional level of complexity. At present, the kinetics of Zn(II) exchange reactions remains mostly unexplored but might prove to be critical for understanding cellular zinc regulation and signaling. Altogether, Zn(II)-selective fluorescent probes have already become an indispensable tool in Zn(II) biology research, and the most recent advances in the development of ratiometric probes offer new exciting opportunities for unraveling the complexity of cellular zinc homeostasis.

Acknowledgments Financial support from the National Science Foundation under grant CHE-1306943 and the National Institutes of Health under the award number R01GM067169 is gratefully acknowledged. We also thank Dr. M. Thomas Morgan for a critical review of the manuscript.

References

Albota MA et al (1998) Two-photon fluorescence excitation cross sections of biomolecular probes from 690 to 960 nm. Appl Opt 37:7352–7356

Baek NY et al (2012) A highly sensitive two-photon fluorescent probe for mitochondrial zinc ions in living tissue. Chem Commun 48:4546–4548

Bourassa D et al (2018) Chromis-1, a ratiometric fluorescent probe optimized for two-photon microscopy reveals dynamic changes in labile Zn(II) in differentiating oligodendrocytes. ACS Sens 3:458–467

Carter KP et al (2014) Fluorescent sensors for measuring metal ions in living systems. Chem Rev 114:4564–4601

Chabosseau P et al (2018) Sensors for measuring subcellular zinc pools. Metallomics 10:229–239

Chang CJ et al (2004) ZP8, a neuronal zinc sensor with improved dynamic range; imaging zinc in hippocampal slices with two-photon microscopy. Inorg Chem 43:6774–6779

Chen YC et al (2015) Photoluminescence imaging of Zn^{2+} in living systems. Chem Soc Rev 44:4517–4546

Cole TB et al (1999) Elimination of zinc from synaptic vesicles in the intact mouse brain by disruption of the ZnT3 gene. Proc Natl Acad Sci U S A 96:1716–1721

Colvin R et al (2010) Cytosolic zinc buffering and muffling: their role in intracellular zinc homeostasis. Metallomics 2:306–317

Danish IA et al (2011) Two-photon probes for Zn^{2+} ions with various dissociation constants. Detection of Zn^{2+} ions in live cells and tissues by two-photon microscopy. Chem Asian J 6:1234–1240

Danscher G (1981) Histochemical-demonstration of heavy-metals - a revised version of the sulfide silver method suitable for both light and electron-microscopy. Histochemistry 71:1–16

Denk W et al (1990) 2-photon laser scanning fluorescence microscopy. Science 248:73–76

Devergnas S et al (2004) Differential regulation of zinc efflux transporters ZnT-1, ZnT-5 and ZnT-7 gene expression by zinc levels: a real-time RT-PCR study. Biochem Pharmacol 68:699–709

Drobizhev M et al (2011) Two-photon absorption properties of fluorescent proteins. Nat Meth 8:393–399

Fahrni C, O'Halloran T (1999) Aqueous coordination chemistry of quinoline-based fluorescence probes for the biological chemistry of zinc. J Am Chem Soc 121:11448–11458

Fahrni C et al (2003) Tuning the photoinduced electron-transfer thermodynamics in 1,3,5-triaryl-2-pyrazoline fluorophores: X-ray structures, photophysical characterization, computational analysis, and in vivo evaluation. J Am Chem Soc 125:3799–3812

Fahrni CJ et al (2017) Probing biological trace metals with fluorescent indicators. In: White AR (ed) Metals in the brain: measurement and imaging, Neuromethods, vol 124. Springer, New York, pp 71–107

Frederickson CJ (1989) Neurobiology of zinc and zinc-containing neurons. Int Rev Neurobiol 31:145–238

Frederickson CJ et al (1987) A quinoline fluorescence method for visualizing and assaying the histochemically reactive zinc (bouton zinc) in the brain. J Neurosci Meth 20:91–103

Gee KR et al (2002a) Measuring zinc in living cells: a new generation of sensitive and selective fluorescent probes. Cell Calcium 31:245–251

Gee KR et al (2002b) Detection and imaging of zinc secretion from pancreatic beta-cells using a new fluorescent zinc indicator. J Am Chem Soc 124:776–778

Grynkiewicz G et al (1985) A new generation of Ca^{2+} indicators with greatly improved fluorescence properties. J Biol Chem 260:3440–3450

Hara T et al (2017) Physiological roles of zinc transporters: molecular and genetic importance in zinc homeostasis. J Physiol Sci 67:283–301

Heinz U et al (2005) On the competition for available zinc. J Biol Chem 280:3197–3207

Hessels AM, Merkx M (2014) Genetically-encoded FRET-based sensors for monitoring Zn^{2+} in living cells. Metallomics 7:258

Hirano T et al (2000) Highly zinc-selective fluorescent sensor molecules suitable for biological applications. J Am Chem Soc 122:12399–12400
Hirano T et al (2002) Improvement and biological applications of fluorescent probes for zinc, ZnAFs. J Am Chem Soc 124:6555–6562
Huang CB et al (2010) Two-photon fluorescence sensors. Prog Chem 22:2408–2419
Hunt JR, Dawlaty JM (2018) Photodriven deprotonation of alcohols by a quinoline photobase. J Phys Chem A 122:7931–7940
Jiang PJ, Guo ZJ (2004) Fluorescent detection of zinc in biological systems: recent development on the design of chemosensors and biosensors. Coord Chem Rev 248:205–229
Jobsis PD et al (2007) Limited utility of acetoxymethyl (AM)-based intracellular delivery systems, in vivo: interference by extracellular esterases. J Microsc 226:74–81
Johnson ID, Spence MTZ (2010) Molecular probes handbook, a guide to fluorescent probes and labeling technologies, 11th edn. Life Technologies
Kambe T et al (2015) The physiological, biochemical, and molecular roles of zinc transporters in zinc homeostasis and metabolism. Physiol Rev 95:749–784
Kamiya M, Johnsson K (2010) Localizable and highly sensitive calcium indicator based on a BODIPY fluorophore. Anal Chem 82:6472–6479
Karim M, Petering D (2016) Newport green, a fluorescent sensor of weakly bound cellular Zn^{2+}: competition with proteome for Zn^{2+}. Metallomics 8:201–210
Khan M et al (2014) Two-photon imaging of Zn^{2+} dynamics in mossy fiber boutons of adult hippocampal slices. Proc Natl Acad Sci USA 111:6786–6791
Kikuchi K et al (2004) Zinc sensing for cellular application. Curr Opin Chem Biol 8:182–191
Kim HM, Cho BR (2011) Two-photon fluorescent probes for metal ions. Chem Asian J 6:58–69
Kim HM, Cho BR (2015) Small-molecule two-photon probes for bioimaging applications. Chem Rev 115:5014–5055
Kim HM et al (2008) Two-photon fluorescent probes for intracellular free zinc ions in living tissue. Angew Chem Int Ed Engl 47:5167–5170
Kiyose K et al (2006) Development of a ratiometric fluorescent zinc ion probe in near-infrared region, based on tricarbocyanine chromophore. J Am Chem Soc 128:6548–6549
Kobat D et al (2009) Deep tissue multiphoton microscopy using longer wavelength excitation. Opt Express 17:13354–13364
Komatsu K et al (2007) Development of an iminocoumarin-based zinc sensor suitable for ratiometric fluorescence imaging of neuronal zinc. J Am Chem Soc 129:13447–13454
Kubin RF, Fletcher AN (1982) Fluorescence quantum yields of some rhodamine dyes. J Lumin 27:455–462
Lan SC, Liu YH (2015) TDDFT study on the excited-state proton transfer of 8-hydroxyquinoline: key role of the excited-state hydrogen-bond strengthening. Spectrochim Acta A 139:49–53
Lee HJ et al (2016) A two-photon fluorescent probe for lysosomal zinc ions. Chem Commun 52:124–127
Li D et al (2015) Genetic targeting of a small fluorescent zinc indicator to cell surface for monitoring zinc secretion. ACS Chem Biol 10:1054–1063
Lim NC, Bruckner C (2004) DPA-substituted coumarins as chemosensors for zinc(II): modulation of the chemosensory characteristics by variation of the position of the chelate on the coumarin. Chem Commun:1094–1095
Lim NC et al (2004) Illuminating zinc in biological systems. Chem Eur J 11:38–49
Liu ZP et al (2014) In vivo ratiometric Zn^{2+} imaging in zebrafish larvae using a new visible light excitable fluorescent sensor. Chem Commun 50:1253–1255
Liu HW et al (2017) Molecular engineering of two-photon fluorescent probes for bioimaging applications. Meth Appl Fluoresc 5:012003
Los GV et al (2008) HaloTag: a novel protein labeling technology for cell imaging and protein analysis. ACS Chem Biol 3:373–382
Loudet A, Burgess K (2007) BODIPY dyes and their derivatives: syntheses and spectroscopic properties. Chem Rev 107:4891–4932

Lu Q et al (2016) Intracellular zinc distribution in mitochondria, ER and the Golgi apparatus. Int J Physiol Pathophysiol Pharmacol 8:35–43
Mahadevan IB et al (1996) The synthesis of Zinquin ester and Zinquin acid, zinc(II)-specific fluorescing agents for use in the study of biological zinc(II). Aust J Chem 49:561–568
Makarov NS et al (2008) Two-photon absorption standards in the 550-1600 nm excitation wavelength range. Opt Express 16:4029–4047
Maret W (2015) Analyzing free zinc(II) ion concentrations in cell biology with fluorescent chelating molecules. Metallomics 7:202–211
Marszalek I et al (2016) Revised stability constant, spectroscopic properties and binding mode of Zn(II) to FluoZin-3, the most common zinc probe in life sciences. J Inorg Biochem 161:107–114
Marszalek I et al (2018) Ternary Zn(II) complexes of FluoZin-3 and the low molecular weight component of the exchangeable cellular zinc pool. Inorg Chem 57:9826–9838
Maruyama S et al (2002) A novel, cell-permeable, fluorescent probe for ratiometric imaging of zinc ion. J Am Chem Soc 124:10650–10651
Masanta G et al (2011) A mitochondrial-targeted two-photon probe for zinc ion. J Am Chem Soc 133:5698–5700
McRae R et al (2009) In situ imaging of metals in cells and tissues. Chem Rev 109:4780–4827
Meeusen J et al (2012) Reaction of metal-binding ligands with the zinc proteome: zinc sensors and *N*,*N*,*N*′,*N*′-tetrakis(2-pyridylmethyl)ethylenediamine. Inorg Chem 51:3625–3632
Morgan MT et al (2019) Ratiometric two-photon microscopy reveals attomolar copper buffering in normal and Menkes mutant cells. Proc Natl Acad Sci U S A 116:12167–12172
Mujumdar RB et al (1993) Cyanine dye labeling reagents: Sulfoindocyanine succinimidyl esters. Bioconjug Chem 4:105–111
Mütze J et al (2012) Excitation spectra and brightness optimization of two-photon excited probes. Biophys J 102:934–944
Nasir M et al (1999) The chemical cell biology of zinc: structure and intracellular fluorescence of a zinc-quinolinesulfonamide complex. J Biol Inorg Chem 4:775–783
Nolan EM, Lippard SJ (2009) Small-molecule fluorescent sensors for investigating zinc metalloneurochemistry. Acc Chem Res 42:193–203
Nowakowski A et al (2015) Chemical-biological properties of zinc sensors TSQ and Zinquin: formation of sensor-Zn-protein adducts versus $Zn(sensor)_2$ complexes. Inorg Chem 54:11637–11647
Pearce DA et al (2001) Derivatives of 8-hydroxy-2-methylquinoline are powerful prototypes for zinc sensors in biological systems. J Am Chem Soc 123:5160–5161
Qin Y et al (2011) Measuring steady-state and dynamic endoplasmic reticulum and Golgi Zn^{2+} with genetically encoded sensors. Proc Natl Acad Sci U S A 108:7351–7356
Qin Y et al (2013) Direct comparison of a genetically encoded sensor and small molecule indicator: implications for quantification of cytosolic Zn^{2+}. ACS Chem Biol 8:2366–2371
Radford RJ et al (2013) Peptide-based targeting of fluorescent zinc sensors to the plasma membrane of live cells (vol 4, pg 3080, 2013). Chem Sci 4:4532–4532
Ricard C et al (2018) Two-photon probes for in vivo multicolor microscopy of the structure and signals of brain cells. Brain Struct Funct 223:3011–3043
Royzen M et al (2005) Ratiometric displacement approach to Cu(II) sensing by fluorescence. J Am Chem Soc 127:1612–1613
Rumi M et al (2000) Structure-property relationships for two-photon absorbing chromophores: Bis-donor diphenylpolyene and bis (styryl) benzene derivatives. J Am Chem Soc 122:9500–9510
Sarkar AR et al (2014) Two-photon fluorescent probes for metal ions in live tissues. Inorg Chem 53:1794–1803
Schießl IM, Castrop H (2016) Deep insights: intravital imaging with two-photon microscopy. Pflugers Arch 468:1505–1516
Sensi SL et al (2003) A new mitochondrial fluorescent zinc sensor. Cell Calcium 34:281–284
Sfrazzetto GT et al (2016) Synthetic fluorescent probes to map metallostasis and intracellular fate of zinc and copper. Coord Chem Rev 311:125–167

Singh H et al (2015) A Golgi-localized two-photon probe for imaging zinc ions. Chem Commun 51:12099–12102
Sjoback R et al (1995) Absorption and fluorescence properties of fluorescein. Spectrochim Acta A 51:L7–L21
Staszewska A et al (2013) Ternary complex formation and competition quench fluorescence of ZnAF family zinc sensors. Metallomics 5:1483–1490
Sumalekshmy S, Fahrni CJ (2011) Metal-ion-responsive fluorescent probes for two-photon excitation microscopy. Chem Mater:823–830
Sumalekshmy S et al (2007) Design of emission ratiometric metal-ion sensors with enhanced two-photon cross section and brightness. J Am Chem Soc 129:11888–11889
Taki M et al (2004) Emission ratiometric imaging of intracellular zinc: design of a benzoxazole fluorescent sensor and its application in two-photon microscopy. J Am Chem Soc 126:712–713
Thompson K et al (2012) Predicting and avoiding subcellular compartmentalization artifacts arising from acetoxymethyl ester calcium imaging probes. The case of fluo-3 AM and a general account of the phenomenon including a problem avoidance chart. Biotech Histochem 87:468–483
Tomat E et al (2008) Organelle-specific zinc detection using zinpyr-labeled fusion proteins in live cells. J Am Chem Soc 130:15776–15777
Tragardh J et al (2015) Exploration of the two-photon excitation spectrum of fluorescent dyes at wavelengths below the range of the Ti:Sapphire laser. J Microsc 259:210–218
Tsien RY (1981) A non-disruptive technique for loading calcium buffers and indicators into cells. Nature 290:527–528
Tsien RY (1988) Fluorescence measurement and photochemical manipulation of cytosolic free calcium. Trends Neurosci 11:419–424
Tsien R, Pozzan T (1989) Measurement of cytosolic free Ca^{2+} with Quin2. Methods Enzymol 172:230–262
Umezawa K et al (2009) Bright, color-tunable fluorescent dyes in the Vis/NIR region: establishment of new "tailor-made" multicolor fluorophores based on borondipyrromethene. Chemistry 15:1096–1106
Vergnano AM et al (2014) Zinc dynamics and action at excitatory synapses. Neuron 82:1101–1114
Vinkenborg JL et al (2009) Genetically encoded FRET sensors to monitor intracellular Zn^{2+} homeostasis. Nat Meth 6:737–740
Walkup GK et al (2000) A new cell-permeable fluorescent probe for Zn^{2+}. J Am Chem Soc 122:5644–5645
Wang C, Yeh AT (2012) Two-photon excited fluorescence enhancement with broadband versus tunable femtosecond laser pulse excitation. J Biomed Opt 17: 025003
Wokosin DL et al (2004) Characterization of a range of fura dyes with two-photon excitation. Biophys J 86:1726–1738
Wommer S et al (2002) Substrate-activated zinc binding of metallo-beta -lactamases: physiological importance of mononuclear enzymes. J Biol Chem 277:24142–24147
Xu C, Webb WW (1996) Measurement of two-photon excitation cross sections of molecular fluorophores with data from 690 to 1050 nm. J Opt Soc Am B 13:481–491
Xu ZC et al (2010) Fluorescent chemosensors for Zn^{2+}. Chem Soc Rev 39:1996–2006
Yao S, Belfield KD (2012) Two-photon fluorescent probes for bioimaging. Eur J Org Chem:3199–3217
Zalewski PD et al (1993) Correlation of apoptosis with change in intracellular labile Zn(II) using zinquin [(2-methyl-8-*p*-toluenesulphonamido-6-quinolyloxy)acetic acid], a new specific fluorescent-probe for Zn(II). Biochem J 296:403–408